Biophysical Journal Volume 106 January 2014 263–271

Surface Characterization of Insulin Protofilaments and Fibril Polymorphs Using Tip-Enhanced Raman Spectroscopy (TERS)

Dmitry Kurouski,[†‡] Tanja Deckert-Gaudig,[§] Volker Deckert,[§¶] and Igor K. Lednev[†*]

[†]Department of Chemistry, University at Albany, SUNY, Albany, New York; [‡]Department of Chemistry, Northwestern University, Evanston, Illinois; [§]Institute of Photonic Technology, Jena, Germany; and [¶]Institute for Physical Chemistry and Abbe Center of Photonics, University of Jena, Jena, Germany

ABSTRACT Amyloid fibrils are β-sheet-rich protein aggregates that are strongly associated with a variety of neurodegenerative maladies, such as Alzheimer's and Parkinson's diseases. Even if the secondary structure of such fibrils is well characterized, a thorough understanding of their surface organization still remains elusive. Tip-enhanced Raman spectroscopy (TERS) is one of a few techniques that allow the direct characterization of the amino acid composition and the protein secondary structure of the amyloid fibril surface. Herein, we investigated the surfaces of two insulin fibril polymorphs with flat (flat) and left-twisted (twisted) morphology. It was found that the two differ substantially in both amino acid composition and protein secondary structure. For example, the amounts of Tyr, Pro, and His differ, as does the number of carboxyl groups on the respective surfaces, whereas the amounts of Phe and of positively charged amino and imino groups remain similar. In addition, the surface of protofilaments, the precursors of the mature flat and twisted fibrils, was investigated using TERS. The results show substantial differences with respect to the mature fibrils. A correlation of amino acid frequencies and protein secondary structures on the surface of protofilaments and on flat and twisted fibrils allowed us to propose a hypothetical mechanism for the propagation to specific fibril polymorphs. This knowledge can shed a light on the toxicity of amyloids and define the key factors responsible for fibril polymorphism. Finally, this work demonstrates the potential of TERS for the surface characterization of amyloid fibril polymorphs.

INTRODUCTION

Protein aggregation inside the human body, which causes the formation of amyloid fibrils, is associated with many neurodegenerative diseases, such as Alzheimer's disease, Parkinson's disease, Huntington's disease, prion diseases, and aging in general. The mechanism of fibril toxicity is not fully understood. According to one hypothesis, fibril aggregates form inside cells as a result of high local protein concentrations in cellular compartments, known as multivesicular bodies (1). The formation of these intracellular aggregates causes cell death leading to the release of toxic fibril species into the extracellular space. According to another hypothesis, the toxicity of amyloid aggregates is associated with fibril-membrane interactions (2,3). Fibrils appear to initiate the disruption of cell membrane structures, causing cell death (4). Alternatively, fibril toxicity could arise from free radical species that are formed on the fibril surface (5,6). According to the hypotheses described previously, the fibril surface is expected to play a significant role in amyloid toxicity (7,8). In addition, amyloid toxicity has been reported to vary with fibril morphology (9–11), which consequently significantly depends on the surface properties and intertwining of protofilaments (12–14).

In vitro aggregation of various amyloid-associated proteins, such as calcitonin (15), amylin (16), transthyretin (17), and mouse prion (9), commonly leads to the formation of two distinct fibril morphologies: a flat tape-like and twisted (18) polymorphs. Microscopic examination of postmortem extracted amyloids from the brains of patients who were diagnosed with Alzheimer's disease also revealed the presence of both of these fibril polymorphs (19,20). It was previously demonstrated that pH determines the morphology, supramolecular chirality, and aggregation mechanisms of insulin fibrils (12).

Insulin is a small protein hormone that consists of 51 amino acid residues organized in two peptide chains linked by disulfide bridges. In rare medical conditions, known as injection amyloidosis, fibrillar aggregates of insulin are found in the derma (21). In vitro insulin aggregation at a pH above 2.4 initially leads to the formation of left-twisted protofilaments. It was found that they intertwine and braid, increasing the magnitude of the twist, and form left-handed fibrils twisted as the final species of the fibrillation process (Fig. 1 *A*) (22). We have recently demonstrated that these twisted insulin fibrils exhibit a distinct vibrational circular dichroism (VCD) spectrum with a sign pattern (+ + - + +), named normal VCD (12). However, low pH (below 2.1) causes the overturn of the protofilament twist direction. These right-twisted protofilaments do not intertwine, but rather associate side by side, forming flat tape-like flat mature fibrils (Fig. 1 *B*) (18). Being formed from right-twisted protofilaments, these flat fibrils exhibit a VCD spectrum that is a mirror image, with respect to the signs, intensities, and peak locations, of the normal VCD. Therefore, a VCD spectrum with a sign pattern (− − + − −) was named reversed

Submitted July 24, 2013, and accepted for publication October 28, 2013.

*Correspondence: ilednev@albany.edu

Editor: David Eliezer.

0006-3495/14/01/0263/9 $2.00

http://dx.doi.org/10.1016/j.bpj.2013.10.040

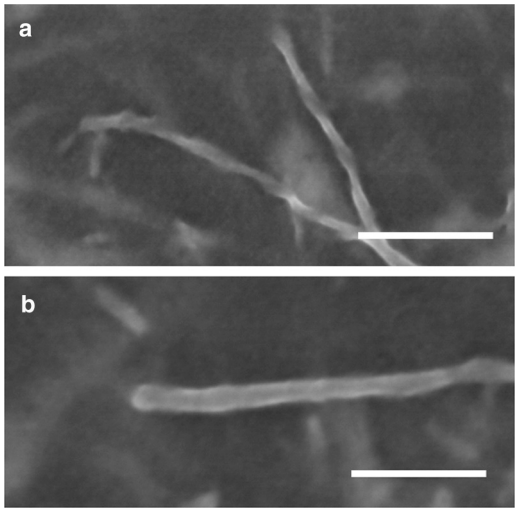

FIGURE 1 SEM images of twisted (*a*) and flat (*b*) insulin fibrils. Scale bar is 100 nm.

VCD (18). The application of deep UV resonance Raman (DUVRR) spectroscopy demonstrated that both chiral polymorphs of insulin fibrils have the same secondary structure of the cross-β core (12). Therefore, it has been proposed that the surface properties of protofilaments and specifically the charge of the carboxyl groups on the surface could play a significant role in their intertwining and the formation of mature fibrils (18).

Amyloid fibrils are noncrystalline and insoluble. This substantially limits the application of classical structural biology tools, such as x-ray crystallography and solution NMR, for determining their structural organization (19,22). Raman spectroscopy, including normal (23,24) and DUVRR (25) spectroscopy, has been used to characterize the structure of amyloid fibrils. These techniques report on the average bulk properties dominated by the contribution from the fibril core. Tip-enhanced Raman scattering (TERS) offers a high depth and lateral spatial resolution in the nanometer range due to the strong field enhancement by the metalized tip of an atomic force microscope (AFM) or scanning tunneling microscope coupled to a Raman spectrometer (26–28). It was demonstrated that using TERS, single-molecule detection can be achieved (29). It was also previously demonstrated that TERS is able to distinguish nucleotide bases and amino acids on the nanoscale (26,30,31).

In our previous study, we applied TERS to characterize the secondary structure and amino acid composition of the surface of twisted insulin fibrils (30) generated at pH 2.5. It was found that their surface is highly heterogeneous and consists of clusters with various protein conformations. According to our data, only ~34% of the surface is dominated by pure β-sheet, whereas the rest is composed of α-helix and unordered protein structures. We also evaluated the frequency of some amino acid residues toward the fibril surface and specific secondary structures on the surface. It appeared that phenylalanine (Phe), tyrosine (Tyr), and cysteine (Cys) are more abundant in the areas with β-sheet structures. Proline (Pro), in contrast, is more often located in areas with α-helix and unordered protein structures. Moreover, analyzing the relative appearance of certain amino acid residues on the fibril surface relative to their overall number in the insulin sequence, we found that Pro has an exceptional frequency to appear at the fibril surface. This observation indicates that Pro is most likely squeezed out of the fibril core upon insulin aggregation. In addition, the fibril surface should be positively charged, as can be concluded from the frequency of amino, imino, and carboxyl groups (30).

In the current study, we employ TERS to examine the secondary structure and amino acid composition of the insulin fibril polymorph surface with flat topology. We compare the surface propensities of Cys, Tyr, Phe, His, and Pro amino acid residues, as well as carboxyl and positively charged amino and imino groups, of twisted and flat fibrils to demonstrate substantial differences in their surface organization. In addition, we investigate the surface of the insulin protofilament precursors of both flat and twisted fibrils with respect to protein secondary structure and amino acid composition. This investigation allows us to propose hypothetical mechanisms of flat and twisted fibril formation and define the amino acid residues responsible for their propagation.

MATERIALS AND METHODS

Insulin fibril preparation

Bovine insulin (Sigma-Aldrich, St. Louis, MO) was dissolved (60 mg/ml) in HCl, pH 2.5 for a formation of twisted or pH 1.5 for growing flat fibril polymorph. The protein solution was heated at 70°C for 2.5 h without stirring. Immediately after fibrillation was complete, an aliquot of the fibrillar gel was resuspended in HCl (pH 2.5 or pH 1.5) solution with a 1:100 dilution factor (V/V). A drop of this suspension was placed onto a precleaned glass (31). After the glass surface was exposed to the fibril suspension for 2–3 min, the solution excess was gently removed, the surface was rinsed with HCl (pH 2.5 or pH 1.5) solution, and dried under an argon flow.

Insulin protofilaments preparation

Bovine insulin (Sigma-Aldrich) was dissolved (60 mg/ml) in HCl, pH 1.5, and the protein solution was heated at 70°C for 20 min. These insulin aggregation conditions were found to be the optimal for gaining the highest yield of insulin protofilaments. It was also demonstrated that mature fibrils are not yet formed at this insulin aggregation stage (18). To prevent their formation, protein aggregation was terminated by immediate temperature drop followed by centrifugation at 20,000 $\times$ *g* for 20 min. The bottom fraction of the centrifuge tube was deposited onto the precleaned glass and exposed on it for 2–3 min. After that, the insulin suspension was removed from the glass surface, which was then rinsed by HCl pH 1.5 and dried under an argon flow.

TERS instrumentation and experiment procedure

Tip-enhanced Raman spectra and fibril AFM images were acquired on a Nanowizard I (JPK Instruments AG, Berlin, Germany) mounted on an

inverted microscope (Olympus IX70, Hamburg, Germany). The following objective conditions were used: oil immersion, 60×, NA = 1,45 (Olympus, Hamburg, Germany), mounted on a Piezo (PIFOC, Physik Instrumente, Karlsruhe, Germany) synchronizing the z-movement of the TERS tip and the laser focus, a confocal Raman spectrometer (LabRam HR, Horiba Jobin Yvon, Villeneuve d'Ascq, France) with a liquid nitrogen-cooled charge-coupled device camera (ISA Spectrum One, Horiba Jobin Yvon, Villeneuve d'Ascq, France), a Krypton ion laser (Innova 300c, wavelength 530,9 nm, Coherent, St. Clara, CA) as the excitation source. Each TERS spectrum was accumulated for 10 s. Spectra were collected from the fibril surface with a lateral distance step that varied from 0.5 to 10 nm. The lateral steps were controlled by an additional 100 × 100 μm sample scanning stage (P-734, Physik Instrumente, Karlsruhe, Germany). To confirm that the TERS tip was not contaminated during the acquisition of spectra of the fibril surface, a reference spectrum from the glass slide was recorded at the end of each measurement. GRAMS/AI 7.0 (Thermo Galactic, Salem, NH) was used for spectral data processing. Spectra shown are raw spectra, no smoothing or baseline correction was applied indicating the high quality of the TERS data.

Scanning electron microscopy (SEM)

For each sample 20 μL of analyzed solution were diluted in 1:400 ratio by in HCl, with a pH at which the sample was aggregated, and deposited on a 200-mesh copper grid. Staining with 1% uranyl acetate was performed in 10 min after the deposition. Samples were imaged on Zeiss Supra SEM in In-Lense mode with 5 kV EHT.

RESULTS AND DISCUSSION

Twisted and flat fibril polymorphs: amino acid composition at the surface

We investigated the surfaces of nine individual twisted fibrils and 17 flat fibrils (AFM topographies are given in the Supporting Material Fig. S1). Detailed topography of the imaged fibrils is hard to achieve with a TERS tip because of a relatively large silver aggregate (20–30 nm in size) on its apex. Nevertheless, the topographies (Fig. S1) reveal clearly the main dimensions of the studied fibril polymorphs.

A total of 162 spectra for twisted (32) and 207 spectra for flat fibrils were collected from fibril surfaces with a step size between 0.5 and 10 nm. The tip and sample positioning were maintained via a closed-loop feedback of the piezo control in the AFM head and the sample stage during the experiment. As the spatial resolution can be also affected by the thermal or mechanical drift, this effect was experimentally evaluated by recording repeatedly the position of some distinct sample features. According to these recordings, the drift was estimated to be <5 nm/h under the typical conditions in our laboratory. Fig. 2 shows spectra that were collected across the main fibril (or protofilament) axis. Two TERS spectra from each polymorph (or protofilament) were recorded in adjacent points on the fibrils surface (from 0.5 to 2 nm), whereas the third one was recorded apart from those two (4 to 10 nm), nevertheless, from the same line across the main fibril (or protofilament) axis. Specifically, spectra ***a*** and ***b*** were acquired 2 nm apart from each other. Spectrum ***c*** was recorded 4 nm from the spectrum ***b***. Spectra

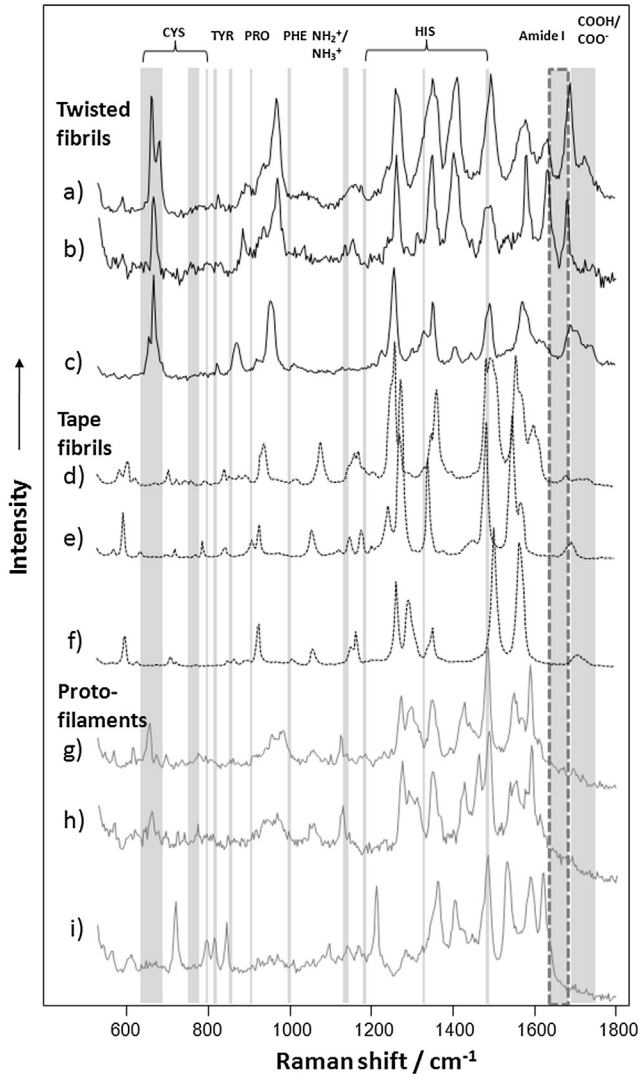

FIGURE 2 Selected TERS spectra acquired from the surfaces of insulin fibril polymorphs and their protofilaments. TERS spectra collected from the surfaces of twisted (—) and flat (· · · ·) fibrils as well as their protofilaments (—). Specific amino acid vibrational modes are marked with gray lines. Amide I bands are marked with dashed lines, showing the borders between protein secondary structures. NH_2/NH_3^+ (1144 cm^{-1}) and $COOH/COO^-$ (1687–1700 cm^{-1}) vibrational modes are also indicated.

d and ***e*** were acquired 1 nm apart from each other. Spectrum ***f*** was recorded 10 nm from the spectrum ***e***. Spectra ***g*** and ***h*** were acquired 0.5 nm apart from each other. Spectrum ***i*** was recorded 6.5 nm from the spectrum ***h***. One can envision that spectra recorded in adjacent points show high similarities, whereas the one acquired from the distant point exhibits substantial deviations with respect to the adjacent ones.

For the current study, amino acids with characteristic marker bands that do not overlap with others and different secondary structures were assessed (shaded). To avoid ambiguous assignment of the vibrational modes in TERS spectra, bands that could be related to more than one amino acid or chemical group are not discussed here (unshaded

spectral regions). The side chains of several amino acids, including Cys, Tyr, Pro, His, and Phe, have characteristic vibrational modes that allow their definite identification (32,33–36). Carboxylic ($COOH/COO^-$), amino and imino (NH_2^+/NH_3^+) groups also have specific bands in TERS spectra (32). The abundances of these characteristic bands in the TERS spectra of twisted and flat fibrils are shown in Fig. 2. Presently, it is not possible to distinguish amino acid residues with saturated hydrocarbon side chains, such as alanine, valine, leucine, and isoleucine because of their spectral similarities.

It is evident from Fig. 3 that the surface of flat fibrils is enriched with Cys (57%) compared to the surface of twisted fibrils (40%). The application of NMR and DUVRR spectroscopy combined with H/D exchange has previously consistently demonstrated that insulin fibril surfaces are highly enriched with Cys (37). Moreover, Cys is organized so that one Cys of each pair (disulfide bond) is located inside the hydrophobic fibril core, although its partner sticks off to the fibril surface (37). It has been proposed that the formation of highly toxic free radical species takes place in the presence of sulfur-containing amino acids and red-ox active transient metal ions, such as Cu and Fe (6). Thus, one can expect that such a high abundance of Cys amino acid residues on the surface of insulin fibrils may possibly be responsible for their high toxicity (38). It is important to mention that although the postmortem examination of patients diagnosed with Alzheimer's disease revealed the presence of fibrils with both flat and twisted topology, it is still not clear which has higher cell toxicity. Based on our data, one can speculate that flat fibrils should be more toxic than the twisted ones.

We found that Tyr, on the other hand, is more common on the surface of twisted fibrils (27%) than on the surface of flat

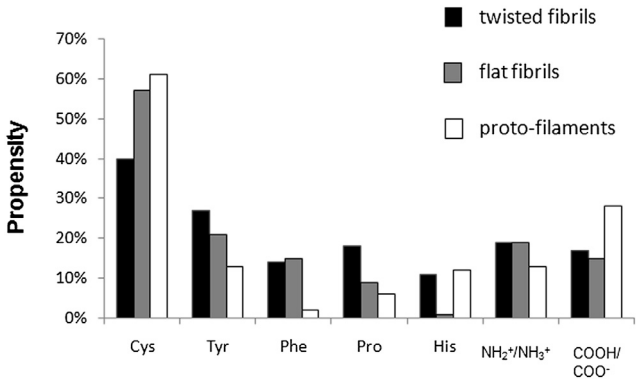

FIGURE 3 Amino acids and charged chemical groups have different frequency presence on the surface of twisted and flat fibril polymorphs as well as their protofilaments. Relative frequency plot of amino acid residues on the surfaces of twisted fibrils (*black*), flat fibrils (*grey*), and their protofilaments (*white*) obtained based on acquired TERS spectra. To obtain the relative frequency, the number of spectra containing a specific amino acid residue was divided by the total number of TERS or SERS spectra in each group. The resulting value was then multiplied by 100 to obtain a percentage. To see this figure in color, go online.

(21%) fibrils. This result is also consistent with our previous DUVRR spectroscopic studies, which revealed substantial differences in the intensities of Tyr bands in the spectra of twisted and flat insulin fibrils (18). Based on our DUVRR data, Tyr amino acid residues are predominantly located in the hydrophobic core rather than on the surface of flat insulin fibrils. By contrast, Tyr has a predominantly hydrophilic local environment (located on the surface) in twisted fibrils. Being on the fibril surface, Tyr is predominantly present in the β-sheet clusters (32).

It was found that Phe is almost equally present on the surfaces of twisted and flat fibrils. The application of DUVRR spectroscopy for the characterization of the secondary structure of twisted and flat insulin fibrils showed that Phe is present in nearly identical local environments in both polymorphs (12).

Proline was found to be rare (9%) on the surface of Flat fibrils, whereas its frequency is twice as high (18%) on the surface of twisted fibrils. This observation suggested that Pro may potentially be squeezed between the protofibrils of flat fibrils, and therefore is out of reach of the extremely surface sensitive TERS.

Raman bands at 1187, 1335, and 1495 cm^{-1} could be assigned to His side-chain vibrations (32). We found that His, like Pro, is very rarely found on the surface of the flat fibrils. Its bands were observed in 1% of the TERS spectra acquired from flat fibrils. However, it is 10 times more common on the surface of twisted fibrils (11%). These results expand our current understanding of His distribution and show that His is not equally distributed on the surfaces of twisted and flat fibrils. Different propensities of Cys, Tyr, Pro, and His amino acid residues on the surface of these fibril polymorphs indicate that these amino acid residues could potentially be involved in determining the formation of one or another insulin fibril polymorph.

The surfaces of twisted and flat fibrils have equal amounts of positively charged amino (NH_3^+) and imino (NH_2^+) groups (19%). In the current study, we assigned carboxyl group ($COOH/COO^-$) presence based on the peak at 1687–1710 cm^{-1} rather than only at 1687 cm^{-1} as we did in our previous work (32). This change was based on several literature reports that describe carboxyl group vibrational modes at 1690–1710 cm^{-1} (39,40). Our data indicate that carboxyl groups have almost equal frequencies on the surfaces of flat and twisted fibrils. Previously, we demonstrated that a small increase in the solution pH results in dramatic structural and morphological changes in flat fibrils (41). It was hypothesized that these changes can be caused by the deprotonation of carboxylic groups, which consequently altered the charge distribution on the fibril surface (42).

To further explore our hypothesis that specific amino acid residues and carboxyl groups can play an important role in the determination of a specific fibril polymorph, we examined the amino acid composition of the surface of protofilaments, the precursors of both twisted and flat insulin fibrils.

Surface of insulin protofilaments

In our previous study, we showed that insulin protofilaments dominate the initial stage (~20 min) of protein aggregation. It was also shown that insulin of both flat and twisted fibrils share the same protofilaments (18). In the current work, an insulin solution at pH 1.5 was heated at 70°C for 20 min, and then rapidly cooled to ~25°C and centrifuged to collect any protofilaments. Using TERS, we investigated the surface of 13 individual protofilaments (selected topologies are shown in Fig. S1). A total of 224 spectra were acquired from their surfaces (Fig. 2), which allowed us to characterize their protein secondary structure (discussed below) and amino acid composition (Fig. 3).

We found that the insulin protofilament surface had a higher amount of carboxyl groups (25%) on the surface than the twisted (17%) and flat (15%) fibrils. This higher frequency of the carboxyl groups indicates that they should become inaccessible by the TERS probe upon insulin fibril propagation (Scheme 1). Such shielding is possible if, in braiding or associating side by side with each other, two protofilaments interact through carboxyl-rich surface areas. In this case, protofilament counterparts, protofibrils, and fibrils would indeed have fewer carboxyl groups on their surface. Therefore, carboxyl groups should be located in the surface areas directly involved in the braiding or side-by-side association of protofilaments. Thus, we conclude that carboxyl groups most likely play an important role in the propagation of protofilaments into fibrils.

Because carboxyl groups are located in the areas of protofilaments' interactions, it becomes crucially important for the further propagation to fibrils whether they are negatively charged or protonated. Negatively charged areas of protofilaments allow them to form twisted mature fibrils. A reduced negative charge on the surface of protofilaments at a pH below 2.1, however, directs their propagation toward the side-by-side association. In this case, flat fibrils are formed (18). These different propagation pathways, which lead to the formation of twisted and flat fibrils finally result in different amounts of carboxyl groups on the surfaces of mature fibrils (Fig. 3). A schematic representation of these two aggregation pathways is shown in our previous study (18).

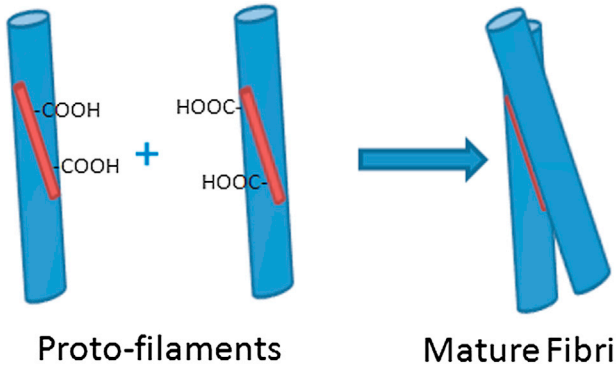

SCHEME 1 A model of carboxyl group integration in the protofilaments' propagation. COOH-rich areas (*red*) of two protofilaments lead to their association and twisted fibril formation.

Insulin protofilaments, in contrast to the previously mentioned carboxylic groups, show only small amounts of Phe and Tyr residues on their surfaces. The amount of Phe on the surface of both twisted and flat fibrils is ~7 times the amount on the surface of protofilaments, and the amount of Tyr is twice as high. This result suggests that these aromatic amino acid residues may also be involved in the propagation of fibrils from protofilaments, as was previously suggested (32).

We found that protofilaments have almost twice the frequency of surface Cys amino acid residues than mature twisted fibrils (61% vs. 40%). This difference suggests that Cys-rich areas of protofilament surfaces pair together, forming mature fibrils. As a result, Cys residues would mainly remain inside the mature fibrils and therefore be inaccessible to TERS (Scheme 1). The latter is consistent with two observations reported previously: i), Cys residues have a strong tendency to appear in β-sheet clusters on the fibril surface; and ii), β-sheet clusters serve as a template for the growth of a new protofilament during the intertwining process (32). At the same time, we found that the prevalence of Cys on the surface of protofilaments is almost equal to its prevalence on flat fibrils (61% and 57%). This result indicates that flat fibrils have a different propagation mechanism that most likely is not associated with Cys pairing upon protofilament aggregation (discussed below). The frequency of His and Pro on the surface of protofilaments also points to a difference in the propagation mechanisms of the flat and twisted forms. For example, the surface of insulin protofilaments is rich in His residues (as in twisted fibrils) and rich in Pro (similar to flat fibrils).

In summary, we can conclude that insulin protofilaments have a surface amino acid composition that is substantially different from both twisted and flat fibrils. They have different frequencies of Phe, Tyr, and COOH/COO^- from both twisted and flat mature fibrils, which suggest that these aromatic amino acid residues and carboxyl groups could be directly involved in the propagation of protofilaments. The differences in the Cys frequency on the surface of protofilaments compared to twisted and flat fibrils suggest that these fibril polymorphs have different formation mechanisms. Finally, the observed deviations in the amino acid composition of fibril and their protofilaments could potentially explain previously observed differences in their toxicity (43).

Twisted and flat fibrils: protein secondary structure

In addition to the amino acid composition, TERS provides information regarding the secondary structural content of an amyloid fibril and its protofilament surface (32). A

protein Raman spectrum is typically composed of contributions from three major types of vibrational mode, which originate from the polypeptide backbone (amide bands) and from aromatic and nonaromatic amino acid residue side chains (44). The position of the amide I bands, which depends on the conformation of the polypeptide backbone and intra- and intermolecular hydrogen bonds, indicates the protein secondary structure (45). The protein secondary structure was assigned as a β-sheet structure if the maximum of the amide I band was between 1664 and 1679 cm^{-1} and as a α-helical/unordered protein structure if the amide I band maximum was observed between 1640 and 1664 cm^{-1} (46). TERS spectra with a broad amide I band that spread over α-helical and β-sheet regions or had two peaks of comparable intensities at 1640–1655 cm^{-1} and 1664–1678 cm^{-1} were then grouped separately and treated as mixtures of all of the protein secondary structures described above. As previously reported, almost half (88 spectra) of all collected TERS spectra from the surface of twisted fibrils (162 spectra) had a suppressed amide I band and therefore could not be used for the interpretation of protein secondary structure. In our previous study, we explained the origin of this phenomenon (47). It was shown that TERS spectra without the amide I band, similar to the ones with it, carry information about the amino acid composition of the analyzed fibril surfaces, and therefore we used them for evaluating the amino acid composition of flat and twisted fibrils (and protofilaments) in our recent study. However, these spectra could not be used to correlate with any protein secondary structure and therefore were excluded for the following data analysis (Fig. 4). A total of 81 and 131 TERS spectra with intense amide I bands were used for the characterization of protein secondary structure of flat fibrils and protofilaments, respectively. It should be noted that from the viewpoint of protein secondary structure we could characterize only those areas of fibril surfaces where amide I was detected in the collected TERS spectra. Apparently, this amount of spectra is sufficient to reveal differences in the secondary structure composition of pH 1.5, pH 2.5 and protofilaments. Currently, there is no other technique capable to detect such information and differences.

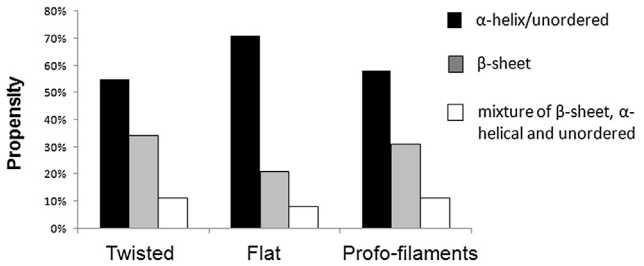

FIGURE 4 Insulin fibril polymorphs and their protofilaments have different composition of protein secondary structures on their surfaces. Relative frequencies of protein secondary structures of the surface of flat and twisted fibril polymorphs as well as their protofilaments: α-helix/unordered (*black*), β-sheet (*gray*), and a mixture of β-sheet, α-helical, and unordered (*white*).

In our previous study, the protein secondary structure composition of twisted fibrils was reported (32). We demonstrated that their surface contains ~55% α-helical and unordered protein structures, although ~34% of the surface is dominated by pure β-sheet protein structures. Approximately 11% of the analyzed TERS spectra revealed a mixture of β-sheet, α-helical, and unordered protein structures. Based on our current data, the surface of flat fibrils contains ~71% α-helical and unordered protein structures, and only 21% is occupied by pure β-sheet protein structures. Approximately 8% of the surface of flat fibrils is composed of a mixture of all these protein structures.

The protein secondary structure of insulin protofilaments is similar to the composition of twisted fibrils. Both are composed of ~58% α-helical and unordered protein structures, although ~31% of the surface is dominated by pure β-sheets. Similar to the twisted fibrils, ~11% of the acquired TERS spectra show a mixture of β-sheet, α-helical, and unordered protein spectral features. The data indicate that the surface of twisted and flat fibrils differ substantially in the protein secondary structure. Approximately a quarter of the surface of flat fibrils is occupied by pure β-sheet, whereas the rest is composed of α-helical and unordered protein structures (71%).

Model of twisted and flat fibril formation

The mechanism of the protofilament propagation into amyloid fibrils is not fully understood. According to one hypothesis, the surface of the protofilament acts as a template for misfolded protein molecules (48). An alternative hypothesis suggests that protofilaments interact (intertwine or associate side by side) with another protofilament, forming protofibrils and finally fibrils (18,49). It was also proposed that β-sheet clusters, located on the surfaces of protofilaments and their counterparts, are involved in the mechanisms described previously. One can envision that, if the amount of β-sheet on the surface decreases from protofilaments to fibrils, their propagation is taking place by the pairing of two protofilaments. In this case, these β-sheet clusters will be located inside the protofilaments' counterparts. At the same time, if the surface of a protofilament is used as a matrix for its replication (template for misfolded protein), the amount of β-sheet should stay the same throughout the protofilaments and fibrils. Our data indicate that the amount of β-sheet remains almost the same on the surface of twisted fibrils compared to protofilaments. This result led us to propose that their formation is taking place through a templating mechanism (Scheme 2). One can imagine that the perfect braiding of such long structures as protofilaments would be associated with some type of steric hindrance. If they were simply braiding as a result of spontaneous surface coadsorption, various loops on their surface, where two protofilaments could not pair up, would be

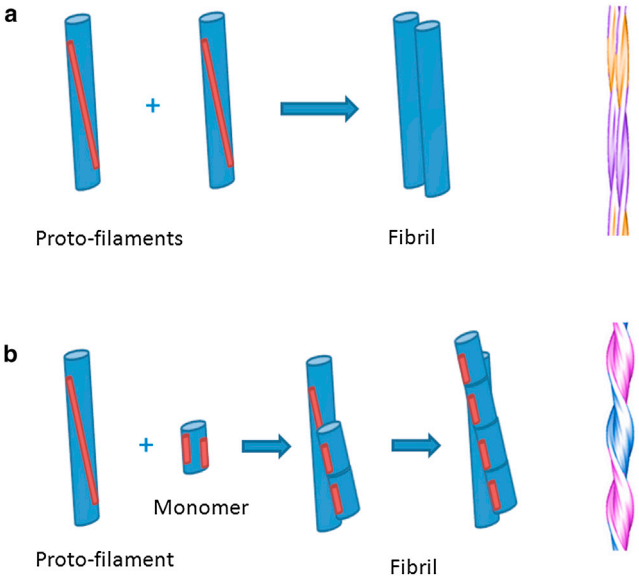

SCHEME 2 Model of flat (*a*) and twisted (*b*) fibril formation. Protofilaments associate side-by-side forming Tape fibrils. Alternatively, surface-driven templating by β-sheet-rich clusters (shown in *red*) leads to the formation of twisted fibrils.

commonly observed. However, such loops were never previously observed (18,49–51).

At the same time, we found that the amount of β-sheet is substantially lower on the surface of flat fibrils compared to their protofilaments. Therefore, it would be expected that the propagation of flat fibrils, if it involves β-sheet domains, is taking place by the pairing of one protofilament with another protofilament. In this case, β-sheet-rich areas would lie inside the interface of the two protofilaments and therefore would no longer be visible for TERS (Scheme 2). Such a surface-driven adhesion of protofilaments, which leads to fibril formation, was previously proposed by Jiménez et al. (50). One can imagine that as a result of this side-by-side association, fibrils may have uneven ends. Indeed, such flat fibrils with uneven ends were previously reported by Jiménez et al. (50).

Summarizing our TERS data allow us to propose different propagation mechanisms for flat and twisted fibril formation. It is important to emphasize that in both cases, the β-sheet-rich hot domains of the protofilament surface drive the fibril formation. The pathway of protofilament propagation, however, is very likely to be determined by the protonation state of the carboxyl groups on their surfaces.

CONCLUSIONS

We performed a detailed surface characterization of insulin fibril chiral polymorphs that exhibit twisted and flat topologies. We found that the two have almost equal amounts of Phe amino acid residues and of positively charged amino and imino groups on the surface. At the same time, the abundance of Tyr, Pro, and His on the surface of twisted fibrils was much higher than on the surface of flat fibrils. Cys, in contrast, is more abundant on the surface of flat fibrils. Flat and twisted fibrils contain nearly equal amounts of carboxyl groups on the surface. At the moment, it is rather unusual to claim that the different compositions of fibril surfaces, as revealed by TERS, determined the morphology of these polymorphs. One can imagine that deviations in amino acid frequencies on their surfaces could simply be a consequence of the different aggregation mechanisms of these fibrils that were described previously. More experimental work is required to define the impact of each specific amino acid on the formation of one or another insulin fibril polymorph.

We also characterized the structural organization and amino acid composition of insulin protofilament surfaces. It was found that they have almost twice the frequency of carboxyl groups on their surfaces compared to the mature fibrils. However, their surfaces contain a very small amount of Tyr and Phe amino acid residues relative to both the flat and the twisted fibrils. Therefore, we conclude that Phe, Tyr, and carboxyl groups are likely to be involved in the propagation mechanism of protofilaments and the formation of mature fibrils. Interestingly, the surface frequency of Cys is almost two times higher for protofilaments than for twisted fibrils and almost equal to its frequency on the surface of flat fibrils. This result suggests that Cys (like Phe, Tyr, and $COOH/COO^{-}$) is potentially involved in the propagation of protofilaments into twisted fibrils but is most likely not involved in the propagation into flat fibrils.

Finally, evaluating the protein secondary structure composition on the surface of twisted and flat fibrils compared to their protofilaments allowed us to conclude that their propagation is taking place by different mechanisms. Flat fibrils are formed as a result of the side-by-side assembly (pairing) of protofilaments, whereas the propagation of twisted fibrils takes place by a surface-templated association of protein monomers.

Overall, this study demonstrates the great potential of TERS for the structural characterization of amyloid fibril polymorphs and the determination of their aggregation pathways. It reveals that understanding the surface amino acid composition and protein secondary structure is extremely valuable for understanding the mechanisms of fibril growth and propagation. Knowledge of the surface composition of amyloid fibrils can be a key for the successful pharmaceutical search for potential drugs that can slow down the progression or prevent the development of various neurodegenerative diseases and maladies associated with protein misfolding.

SUPPORTING MATERIAL

One figure is available at http://www.biophysj.org/biophysj/supplemental/S0006-3495(13)02378-3.

This project is supported by Award No. R01AG033719 from the National Institutes of Health (I.K.L.).

REFERENCES

1. Friedrich, R. P., K. Tepper, …, M. Fändrich. 2010. Mechanism of amyloid plaque formation suggests an intracellular basis of Abeta pathogenicity. *Proc. Natl. Acad. Sci. USA.* 107:1942–1947.
2. Matsuzaki, K., K. Kato, and K. Yanagisawa. 2010. Abeta polymerization through interaction with membrane gangliosides. *Biochim. Biophys. Acta.* 1801:868–877.
3. Jarrett, J. T., and P. T. Lansbury, Jr. 1993. Seeding "one-dimensional crystallization" of amyloid: a pathogenic mechanism in Alzheimer's disease and scrapie? *Cell.* 73:1055–1058.
4. Huang, B., J. He, …, C. M. Zeng. 2009. Cellular membrane disruption by amyloid fibrils involved intermolecular disulfide cross-linking. *Biochemistry.* 48:5794–5800.
5. Kay, C. J. 1997. Mechanochemical mechanism for peptidyl free radical generation by amyloid fibrils. *FEBS Lett.* 403:230–235.
6. Pogocki, D. 2003. Alzheimer's beta-amyloid peptide as a source of neurotoxic free radicals: the role of structural effects. *Acta Neurobiol. Exp. (Warsz.).* 63:131–145.
7. Heredia, L., R. Lin, …, A. Lorenzo. 2004. Deposition of amyloid fibrils promotes cell-surface accumulation of amyloid beta precursor protein. *Neurobiol. Dis.* 16:617–629.
8. Stefani, M. 2010. Structural polymorphism of amyloid oligomers and fibrils underlies different fibrillization pathways: immunogenicity and cytotoxicity. *Curr. Protein Pept. Sci.* 11:343–354.
9. Anderson, M., O. V. Bocharova, …, I. V. Baskakov. 2006. Polymorphism and ultrastructural organization of prion protein amyloid fibrils: an insight from high resolution atomic force microscopy. *J. Mol. Biol.* 358:580–596.
10. Seilheimer, B., B. Bohrmann, …, H. Döbeli. 1997. The toxicity of the Alzheimer's beta-amyloid peptide correlates with a distinct fiber morphology. *J. Struct. Biol.* 119:59–71.
11. Lührs, T., C. Ritter, …, R. Riek. 2005. 3D structure of Alzheimer's amyloid-beta(1-42) fibrils. *Proc. Natl. Acad. Sci. USA.* 102:17342–17347.
12. Kurouski, D., R. A. Lombardi, …, L. A. Nafie. 2010. Direct observation and pH control of reversed supramolecular chirality in insulin fibrils by vibrational circular dichroism. *Chem. Commun. (Camb.).* 46:7154–7156.
13. Heldt, C. L., D. Kurouski, …, G. Belfort. 2011. Isolating toxic insulin amyloid reactive species that lack β-sheets and have wide pH stability. *Biophys. J.* 100:2792–2800.
14. Adamcik, J., and R. Mezzenga. 2011. Adjustable twisting periodic pitch of amyloid fibrils. *Soft Matter.* 7:5437–5443.
15. Bauer, H. H., U. Aebi, …, H. P. Merkle. 1995. Architecture and polymorphism of fibrillar supramolecular assemblies produced by in vitro aggregation of human calcitonin. *J. Struct. Biol.* 115:1–15.
16. Goldsbury, C. S., G. J. Cooper, …, J. Kistler. 1997. Polymorphic fibrillar assembly of human amylin. *J. Struct. Biol.* 119:17–27.
17. Cardoso, I., C. S. Goldsbury, …, M. J. Saraiva. 2002. Transthyretin fibrillogenesis entails the assembly of monomers: a molecular model for in vitro assembled transthyretin amyloid-like fibrils. *J. Mol. Biol.* 317:683–695.
18. Kurouski, D., R. Dukor, …, I. K. Lednev. 2012. Normal and reversed supramolecular chirality of insulin fibrils probed by vibrational circular dichroism at the protofilament level of fibril structure. *Biophys. J.* 103:522–531.
19. Paravastu, A. K., R. D. Leapman, …, R. Tycko. 2008. Molecular structural basis for polymorphism in Alzheimer's beta-amyloid fibrils. *Proc. Natl. Acad. Sci. USA.* 105:18349–18354.
20. Wischik, C. M., M. Novak, …, A. Klug. 1988. Isolation of a fragment of tau derived from the core of the paired helical filament of Alzheimer disease. *Proc. Natl. Acad. Sci. USA.* 85:4506–4510.
21. Dische, F. E., C. Wernstedt, …, P. J. Watkins. 1988. Insulin as an amyloid-fibril protein at sites of repeated insulin injections in a diabetic patient. *Diabetologia.* 31:158–161.
22. Ivanova, M. I., S. A. Sievers, …, D. Eisenberg. 2009. Molecular basis for insulin fibril assembly. *Proc. Natl. Acad. Sci. USA.* 106:18990–18995.
23. Dong, J., Z. Wan, …, M. A. Weiss. 2003. Insulin assembly damps conformational fluctuations: Raman analysis of amide I linewidths in native states and fibrils. *J. Mol. Biol.* 330:431–442.
24. Ortiz, C., D. Zhang, …, D. Ben-Amotz. 2007. Analysis of insulin amyloid fibrils by Raman spectroscopy. *Biophys. Chem.* 128:150–155.
25. Oladepo, S. A., K. Xiong, …, I. K. Lednev. 2012. UV resonance Raman investigations of peptide and protein structure and dynamics. *Chem. Rev.* 112:2604–2628.
26. Deckert-Gaudig, T., and V. Deckert. 2011. Nanoscale structural analysis using tip-enhanced Raman spectroscopy. *Curr. Opin. Chem. Biol.* 15:719–724.
27. Stadler, J., T. Schmid, and R. Zenobi. 2012. Developments in and practical guidelines for tip-enhanced Raman spectroscopy. *Nanoscale.* 4:1856–1870.
28. Jiang, N., E. T. Foley, …, R. P. Van Duyne. 2012. Observation of multiple vibrational modes in ultrahigh vacuum tip-enhanced Raman spectroscopy combined with molecular-resolution scanning tunneling microscopy. *Nano Lett.* 12:5061–5067.
29. Sonntag, M. D., J. M. Klingsporn, …, R. P. Van Duyne. 2012. Single molecule tip enhanced Raman spectroscopy. *J. Phys. Chem. C.* 116:478–483.
30. Deckert-Gaudig, T., and V. Deckert. 2010. Tip-enhanced Raman scattering (TERS) and high-resolution bio nano-analysis—a comparison. *Phys. Chem. Chem. Phys.* 12:12040–12049.
31. Deckert-Gaudig, T., E. Kämmer, and V. Deckert. 2012. Tracking of nanoscale structural variations on a single amyloid fibril with tip-enhanced Raman scattering. *J. Biophotonics.* 5:215–219.
32. Kurouski, D., T. Deckert-Gaudig, …, I. K. Lednev. 2012. Structure and composition of insulin fibril surfaces probed by TERS. *J. Am. Chem. Soc.* 134:13323–13329.
33. Budich, C., U. Neugebauer, …, V. Deckert. 2008. Cell wall investigations utilizing tip-enhanced Raman scattering. *J. Microsc.* 229: 533–539.
34. Deckert-Gaudig, T., E. Bailo, and V. Deckert. 2009. Tip-enhanced Raman scattering (TERS) of oxidized glutathione on an ultraflat gold nanoplate. *Phys. Chem. Chem. Phys.* 11:7360–7362.
35. Deckert-Gaudig, T., and V. Deckert. 2009. Ultraflat transparent gold nanoplates—ideal substrates for tip-enhanced Raman scattering experiments. *Small.* 5:432–436.
36. Deckert-Gaudig, T., and V. Deckert. 2009. Tip-enhanced Raman scattering studies of histidine on novel silver substrates. *J. Raman Spectrosc.* 40:1446–1451.
37. Kurouski, D., J. Washington, …, I. K. Lednev. 2012. Disulfide bridges remain intact while native insulin converts into amyloid fibrils. *PLoS ONE.* 7:e36989.
38. Shivaprasad, S., and R. Wetzel. 2006. Scanning cysteine mutagenesis analysis of Abeta-(1-40) amyloid fibrils. *J. Biol. Chem.* 281:993–1000.
39. Picquart, M., L. Grajcar, …, Z. Abedinzadeh. 1999. Vibrational spectroscopic study of glutathione complexation in aqueous solutions. *Biospectroscopy.* 5:328–337.
40. Edsall, J. T. 1937. Raman spectra of amino acids and related compounds IV. Ionization of di- and tricarboxylic acids. *J. Chem. Phys.* 5:508–518.
41. Kurouski, D., R. K. Dukor, …, I. K. Lednev. 2012. Spontaneous inter-conversion of insulin fibril chirality. *Chem. Commun. (Camb.).* 48:2837–2839.
42. Darrington, R. T., and B. D. Anderson. 1995. Evidence for a common intermediate in insulin deamidation and covalent dimer formation: effects of pH and aniline trapping in dilute acidic solutions. *J. Pharm. Sci.* 84:275–282.

43. Zako, T., M. Sakono, …, M. Maeda. 2009. Bovine insulin filaments induced by reducing disulfide bonds show a different morphology, secondary structure, and cell toxicity from intact insulin amyloid fibrils. *Biophys. J.* 96:3331–3340.

44. Lednev, I. K. 2007. Vibrational spectroscopy: biological applications of ultraviolet Raman spectroscopy. *In* Protein Structures, Methods in Protein Structures and Stability Analysis. V. N. Uversky and E. A. Permyakov, editors. Nova Science, Hauppauge, NY, pp. 1–26.

45. Carey, P. R. 1982. Biochemical Applications of Raman and Resonance Raman Spectroscopies. Academic Press, New York.

46. Fabian, H., and P. Anzenbacher. 1993. New developments in Raman spectroscopy of biological systems. *Vib. Spectrosc.* 4:125–148.

47. Kurouski, D., T. Postiglione, …, I. K. Lednev. 2013. Amide I vibrational mode suppression in surface (SERS) and tip (TERS) enhanced Raman spectra of protein specimens. *Analyst (Lond.).* 138:1665–1673.

48. Milhiet, P. E., D. Yamamoto, …, T. Ando. 2010. Deciphering the structure, growth and assembly of amyloid-like fibrils using high-speed atomic force microscopy. *PLoS ONE.* 5:e13240.

49. Jansen, R., W. Dzwolak, and R. Winter. 2005. Amyloidogenic self-assembly of insulin aggregates probed by high resolution atomic force microscopy. *Biophys. J.* 88:1344–1353.

50. Jiménez, J. L., E. J. Nettleton, …, H. R. Saibil. 2002. The protofilament structure of insulin amyloid fibrils. *Proc. Natl. Acad. Sci. USA.* 99:9196–9201.

51. Khurana, R., C. Ionescu-Zanetti, …, S. A. Carter. 2003. A general model for amyloid fibril assembly based on morphological studies using atomic force microscopy. *Biophys. J.* 85:1135–1144.

52. Reference deleted in proof.